In situ transcriptional profile of a germinal center plasmablastic burst hints at an unfavorable Diffuse Large B-cell Lymphoma subset.

Vincenzo L'Imperio[1]*, Gaia Morello[2]*, Valeria Cancila[2], Giorgio Bertolazzi[2], Saveria Mazzara[3], Beatrice Belmonte[2], Piera Balzarini[4], Lilia Corral[5], Arianna Di Napoli[6], Fabio Facchetti[7], Fabio Pagni[1]*, Claudio Tripodo[2,8]*

[1] Department of Medicine and Surgery, University of Milano-Bicocca, Pathology, San Gerardo Hospital, Via G.B. Pergolesi 33, Monza, Italy.
[2] Tumor Immunology Unit, Department of Sciences for Health Promotion and Mother-Child Care "G. D'Alessandro", University of Palermo, Palermo, Italy.
[3] Division of Diagnostic Haematopathology, European Institute of Oncology, Milan, Italy.
[4] Department of Molecular and Translational Medicine, University of Brescia, Piazzale Spedali Civili 1, 25123, Brescia, Italy.
[5] Centro Ricerca Tettamanti, Pediatric Clinic, University of Milan Bicocca, San Gerardo Hospital/Fondazione MBBM, Monza, Italy.
[6] Pathology Unit, Sapienza University of Rome, Sant'Andrea Hospital, Rome, Italy.
[7] Pathology Unit, University of Brescia, Brescia, Italy.
[8] Tumor and Microenvironment Histopathology Unit, IFOM, the FIRC Institute of Molecular Oncology, Milan, Italy.

* These Authors equally contributed

Correspondence:

Prof. Claudio Tripodo, Tumor Immunology Unit, University of Palermo, Corso Tukory 211, 90134, Palermo. Phone +3909123896211. Email: claudio.tripodo@unipa.it

Abstract

The germinal center (GC) reaction results in the selection of B-cells acquiring effector Ig secreting ability by progressing towards plasmablastic differentiation. This transition is associated with exclusion from the GC microenvironment. The aberrant expansion of plasmablastic elements within the GC fringes configures an atypical condition, the biological characteristics of which have not been defined yet. We investigated the *in situ* immunophenotypical and transcriptional characteristics of a non-clonal germinotropic expansion of plasmablastic elements (GEx) occurring in the tonsil of a young patient. Compared to neighboring GC and peri-follicular regions, the GEx showed a distinctive signature featuring key regulators of plasmacytic differentiation, cytokine signaling, and cell metabolism. The GEx signature was tested in the setting of diffuse large B-cell lymphoma (DLBCL) as a prototypical model of lymphomagenesis encompassing transformation at different stages of GC and post-GC functional differentiation. The signature outlined DLBCL clusters with different overall survival, highlighting the negative prognostic significance of the overexpression of hallmark genes of this peculiar condition.

Running title: Spatial profiling of a germinotropic plasmablastic expansion

Keywords: digital spatial profiling, germinal center, plasmablast, diffuse large B-cell lymphoma.

Introduction

Within secondary lymphoid organs immune cells display topographic compartmentalization underlying functional commitment towards different stages of immune response induction and regulation. In lymphoid follicles, germinal centers (GCs) represent a complex specialized microenvironment sustaining B-cell proliferative bursts underlying somatic hypermutation and class-switch recombination of immunoglobulin (Ig) genes, communication with T cell subsets with helping function (Tfh), and interplay with specialized mesenchymal scaffolds (i.e. FDCs) (1). These events play through the dynamical iteration of elements between the dark (DZ), intermediate and light (LZ) zones of the GC (2), eventually resulting in the differentiation and displacement from the GC of cells acquiring effector capabilities through the synthesis and secretion of Igs (i.e. plasmablasts and plasma cells) (3). Alterations in the topographic compartmentalization of GC and extra-GC populations in lymphoid tissues are commonly observed in the setting of lymphoproliferative diseases, where the accumulation of cells with morphological or immunophenotypical features conflicting with their topographic localization represents a hallmark of histopathological analyses. This assumption reached its highest expression with the introduction of a diffuse large B cell lymphoma (DLBCL) prognostic sub-classification based on the presumed cell-of-origin (COO), as determined by gene expression profiling (GEP) (4-6).

We have investigated here an atypical germinotropic expansion of non-clonal, light-chain restricted B cells with plasmablastic features confined to a single enlarged GC structure in the tonsil of a young patient, through in situ immunolocalization analyses and high throughput digital spatial profiling. Comparing the features of the atypical germinotropic expansion (GEx) with those of topographically preserved DZ, LZ and peri-follicular (PERI) regions of interest (ROIs) we identified a unique transcriptomic profile of the GEx ROIs featuring the

overexpression of transcripts involved in plasmacytoid differentiation, cytokine signaling, and cell metabolism.

To probe the reflection of the identified transcriptional signature in a setting of B-cell lymphomatous transformation embracing the full spectrum of GC- and post-GC differentiation, the discriminative 20 genes were used to cluster a large cohort of diffuse large B-cell lymphoma (DLBCL) transcriptomic data. The GEx signature highlighted two clusters with different overall survival in DLBCL, where cases with the highest expression of GEx hallmark genes were characterized by poorer prognosis.

Materials and methods

Clinical setting

This study started from the incidental finding of the reactive germinotropic plasmablastic expansion described in the Results section, in the tonsil of a young patient who underwent tonsillectomy for clinical hypertrophy. Sample was obtained and handled according to the Declaration of Helsinki. Informed consent for surgery and histopathological studies was obtained from the legal representatives. The case was included in the study 05/2018 approved by the University of Palermo Institutional Review Board.

Histological, immunohistochemical and molecular analyses

Tonsillar tissue has been formalin-fixed and paraffin-embedded (FFPE) and 3 μm thick sections have been stained with hematoxylin and eosin (H&E). IHC has been performed at the Pathology Department of ASST Monza, San Gerardo Hospital, Monza, Italy using a Dako Omnis platform (Dako, Denmark) using antibodies directed against CD20 (L26), CD3 (Polyclonal), Bcl2 (124), Bcl6 (PG-B6p), CD21, ki-67 (Mib-1), MUM1, CD10, CD30 (Ber-H2), CD138 (Mi15), HHV8 (13B10), kappa and lambda light chains. Double

immunohistochemistry has been performed for MUM1 and CD10 using 3-3'-diaminobenzidine (DAB) and 3-amino-9-ethylcarbazole (AEC) as chromogens, respectively. In situ fluorescence hybridization (FISH) study has been performed using a IRF4/DUSP22 (6p25) Break Apart kit (Kreatech, Leica Biosystem, Germany) at the Pathology Department of Spedali Riuniti di Brescia. Quantitative evaluation of immunophenotypical markers was performed by applying the HALO image analysis software (v3.2.1851.229, Indica Labs) to regions selected on whole slide digital scans acquired using an Aperio CS2 slide scanner with the ImageScope software (v12.3.28013, Leica Biosystems, Germany).

Quantitative polymerase chain reaction (Q-PCR) to detect clonal immunoglobulin genes rearrangement was performed after laser microdissection on H&E-stained slides, using an LMD6 platform (Leica Microsystems, Germany).

Digital spatial profiling

The transcriptional landscape of 15 different spatially-resolved regions of interests (ROIs) of the tonsil (5 peri/inter-follicular ROIs, 5 DZ and 5 LZ ROIs from morphologically normal follicles) and 9 ROIs from the GEx was determined by Digital Spatial Profiling on slides stained with CD271/NGFR (as an FDC marker to highlight the LZ) and CD20 (as a B-cell marker). The 24 selected and segmented ROIs were profiled using a GeoMx Digital Spatial Profiler (DSP) (NanoString, Seattle WA) as previously described (7), applying the Cancer Transcriptome Atlas panel (https://www.nanostring.com/products/geomx-digital-spatial-profiler/geomx-rna-assays/geomx-cancer-transcriptome-atlas/) (Supplementary Table 1).

Bioinformatic Data Analysis

After quality check step, raw counts were normalized against the 75th percentile of signal from their own ROI and normalized data were used to perform PCA using FactoMine R package. For hierarchical clustering analysis of the ROIs the Euclidean distance metric across samples

was considered and complete aggregation method was used for building tree within the R package hclust.

Differential expression analyses were carried out by applying the moderated t-test using the limma package (8); pairwise comparisons between GEx and DZ/LZ/Peri ROIs were considered. Upregulated/downregulated genes were selected for subsequent analysis if their expression values were found to exceed the threshold of 0.05 FWER (Bonferroni correction).

The spatial GEx signature was assessed in the following GEO datasets: GSE32918 (9) and GSE117556 (10). First, samples with a low Pearson correlation coefficient with other samples in the space of all genes for each separately dataset were removed as proposed by Kotlov et al.(28). Probe sets were annotated using the annotation files from IlluminaHumanv4.db and illumina Humanv3.db . When multiple probes were associated to the same we collapsed to the average value. Next, the two transcriptomic datasets were combined and a quantile normalization was performed using preprocess Core package. Furthermore, possible batch effects were corrected with limma package and a PCA was considered to verify the effective removal of the batch effects.

The clinical information for rGSE32918 cohort (9) was downloaded from GEO repository while, forGSE117556 cohort was retrieved from the supplementary material of Sha et al (10).

After performing z-score, unsupervised hierarchical clustering analysis based on the GEx signature was applied to identify potential discriminative clusters based on Ward.D2 method on the Euclidean distance of z-score expression. Silhouette and the elbow methods, from the factoextra R package were employed to choose the optimal number of clusters. Differences in the total GEx signature expression inside clusters were evaluated using a Kolmogorov-Smirnov test on ECDFs. The Cox model has been fitted to estimate the relative risk of death between clusters. Before calculating the log-rank test and fitting the Cox model, the cox.pzh test has

been used to test the proportional hazard assumption. In order to directly evaluate the association between patient survival time and expression of the GEx signature, we assessed a quantile strategy to split patients into four groups. To analyze the prognostic value of GEx signature, merged cohort was dichotomized into higher (GEx expression is greater than the 75th quantile) and lower groups (GEx expression is lower than the 25th quantile) whereas patients with the GEx expression between the two extremes were excluded from the survival analysis. Difference in patient characteristics was analyzed with the Fisher's exact test.

All statistical analyses were performed using R statistical software (v4.0.2, http://www.R-project.org).

Data Availability

Normalized gene expression data generated in the Digital Spatial Profiling experiment are available in Supplementary Table 1

Results

Pathology of the tonsil

Histopathological analysis of the left tonsil from a young patient with clinical bilateral hypertrophy revealed, in a background of lymphoid follicles with hyperplastic features and preserved GC DZ, LZ and mantles, an isolated abnormal follicle with flattened mantle zone, an enlarged GC, without evident DZ/LZ polarization, preservation of rare tingible body macrophages, and populated by a predominance of monomorphic plasmacytoid cells with immature morphology (Figure 1A). Quantitative immunophenotypical characterization of reactive follicular and peri-follicular regions and of the atypical germinotropic plasmablasts (GEx), highlighted conspicuous differences in the immune profile (Figure 1B-C). The reactive

178 preserved DZ and LZ of GCs were characterized by B cells with strong CD20 expression, dense
179 Ki-67 immunoreactivity (higher in the DZ), negativity for IRF4, except for scattered cells in a
180 background of CD10-expressing cells, Bcl-2 negativity, slight T-cell infiltration (denser in the
181 LZ), and no evidence of light chain restriction (Figure 1B-C). At contrast, the composition of
182 the GEx displayed a CD20+ B cell phenotype, high Ki-67+ proliferative fraction, diffuse IRF4
183 positivity with IRF4+ cells co-expressing CD10, negativity for Bcl-2, and
184 immunophenotypical restriction for lambda light chain (Figure 1B-C). Most of the cells
185 populating the GEx also expressed CD138 in the absence of CD30, indicating partial
186 acquisition of a plasmablastic phenotype. Immunoistochemistry for HHV8 and *in situ*
187 hybridization for EBER (EBV) proved negative (Supplementary Figure 1). On the basis of the
188 GEx lambda light chain restriction, analysis of the Ig light and heavy genes rearrangement was
189 performed on DNA extracted by laser microdissection of the GEx, which revealed a polyclonal
190 profile (Supplementary Figure 2). The strong and diffuse immunoreactivity of IRF4 and the
191 co-occurrence of IRF4/CD10 double-expressing elements prompted the analysis of *IRF4* gene
192 rearrangement by fluorescence in situ hybridization (FISH), which did not reveal any
193 abnormality (Supplementary Figure 3), allowing to exclude an IRF4-rearranged lymphoma.
194
195 *Digital Spatial Profiling of the GEx regions reveals a distinctive profile*
196 The molecular profiles of non-malignant GC compartments can be exploited to probe GC
197 microenvironment imprints in B-cell lymphomas with different degree of relationship with GC
198 subpopulations, such as DLBCL, in which the COO has shown prognostic significance in the
199 setting of standard chemo-immunotherapy regimens (7). We had the opportunity to probe the
200 in situ transcriptional profile of a yet unexplored atypical configuration of a GC proliferative
201 burst. Through the Nanostring GeoMx technology, the expression of 1824 genes from key
202 cancer-associated transcriptional programs (Supplementary Table 1) was determined on 5 DZ,

5 LZ and 5 PERI ROIs selected from morphologically/phenotypically preserved follicles/perifollicular areas, and on 9 GEx ROIs. We then asked whether GEx ROIs could be defined by a specific gene signature; to this aim, principal component analysis (PCA) and unsupervised hierarchical clustering were investigated. PCA revealed that ROIs segregated according to their spatial classification, with PERI regions showing neatly separated profiles from GC ROIs including DZ, LZ and GEx and GEx ROIs clustered together with other GC regions, showing some degree of intermixing with LZ ROIs (Figure 2A). Consistently, clustering analysis confirmed the same degree of relationship between the different ROIs (Figure 2B). mRNA expression of the transcripts relative to the IHC markers evaluated for quantitative immunopehnotypical analyses showed consistency with the protein expression pattern (Supplementary Figure 4). Pairwise differential expression analysis performed on the different ROIs allowed to identify candidate genes reflecting the distinctive profiles between the GEx ROIs in comparison with DZ LZ and PERI ROIs (Figure 2C-F). Among the 20 genes, 17 were significantly upregulated in GEx ROIs, while 3 were downmodulated (Figure 2C-F). GEx hallmark genes included, along with the plasma cell differentiation markers *PRDM1*, *IRF4*, *TNFRSF17* (BCMA) and *CD9*, genes involved in 2-oxoglutarate metabolism (*GOT2*, *IDH2)*, in IL17 pathway (*IL17RB, HSP90B1*) and cytokine signaling (*RASAL1*, *LTB*), in PI3K-Akt pathway (*SGK1, BCL2L1*), in lymphocyte activation (*ADA*, *SCL7A5, FCRL2*) and cell surface regulation of immune activation (*CD24, LILRB1*), in cell adhesion (*ANKRD28*) and response to abiotic (i.e. osmotic) stress (*SLK1*). Moreover, the long non-coding RNA *FAM30* was also listed among the GEx hallmarks.

The GEx signature outlines a subset of DLBCL with unfavorable prognosis

To investigate whether the transcriptional hallmarks identified in the GEx ROIs could be traced in the heterogeneous spectrum of B-cell malignant transformation recapitulated by DLBCL,

we applied the GEx gene signature to a harmonized dataset of 1147 DLBCL cases relative to GSE32918 (9) and GSE117556 (10). Based on the expression of the GEx signature (19 protein-coding genes), DLBCL clustered into two main groups (Figure 3A), with the cluster 1 characterized by significantly different enrichment in ABC cases (Fisher exact test p-value < 10e-10) and significantly worst overall survival (Figure 3A-B, relative risk (RR) = 1.61, p-val < 0.001). Since 17 out of the 20 GEx differential genes were overexpressed as compared with DZ, LZ, and PERI ROIs, we comparatively analyzed DLBCL cases expressing high or low levels of the GEx overexpressed genes focusing on the Q1 and Q4 quartiles of their cumulative expression (Figure 3C). DLBCL cases characterized by highest (Q4) cumulative expression of the GEx genes had a significantly poorer OS as compared with cases characterized by the lowest expression (Q1) (Figure 3C, RR = 1.63, p-value = 0.002). The negative prognostic value of the GEx overexpressed genes was significant also when ABC DLBCL cases only were considered (Figure 3D, RR = 1.79, p-val = 0.04), while it was lost in the GCB DLBCL subset (Figure 3E, RR = 1.22, p-val = 0.37), suggesting that the genes positively characterizing GEx ROIs underlie a specific biology related with the ABC COO, known to be enriched in clones undergoing plasmablastic/plasmacytic commitment.

Discussion

Plasma cells (PCs) represent the final step of the functional differentiation process of the B lymphocyte, through the transition in short-living highly proliferative plasmablasts. The transition of B cells undergoing selection and refinement of their IG receptor in the GC reaction towards effectors capable of Ig secretion implies the acquisition of plasmablastic/plasmacytoid features within the GC microenvironment. The spatial localization of these functional and phenotypical intermediates is still poorly characterized and depends on the dynamical modulation of chemotactic receptor/ligand axes interweaving with BCR-controlled programs

(11). Proliferating cells with plasmablastic/plasmacytoid features accumulating within the GC therefore represents an element of atypia even in the setting of non-clonal events, and little is known about the *molecular signature* characterizing their transient state (12). In this report we phenotypically and transcriptionally characterized an immunoglobulin light chain restricted non-clonal atypical germinotropic expansion of plasmablastic cells, investigating differential features emerging from the comparison with neighboring GC and extra-GC regions. The GEx ROIs were characterized by the unique co-occurrence of IRF4 and CD10 expression, which highlighted a transitory state engendered by IRF4 control of GC exit (13) and CD10 ectopeptidase retention that can be observed in DLBCL with plasmablastic differentiation (14). On digital spatial profiling, a set of 20 genes were found differentially expressed in GEx ROIs as compared with neighboring DZ, LZ and PERI ROIs. The discriminating signature resulted positively enriched in the key transcription factors driving plasma cell differentiation IRF4 and PRDM1, and included the B-cell differentiation receptor BCMA involved in the transduction of trophic signals from APRIL and BAFF tumor necrosis factor superfamily ligands (15). Such molecular features supportive of a plasmablastic phenotype were also supported by the downregulation of CD24, a signal transducer negatively modulated in response to BCR activation and along plasmablastic transition (16). The GC localization of the plasmablastic expansion found resonance in the overexpression of CD9. The tetraspanin CD9 has been reported to mark a subset of B cells in the human GC characterized by plasmablastic differentiation and Blimp1 (*PRDM1*) expression (17). These CD9+ GC B cells more efficiently give rise to CD20-CD38+ plasmablasts as compared with their CD9- counterpart. Moreover, in the murine setting, the efficient plasmablastic/plasmacytic differentiation of CD9+ B cells is shared by non-GC B-cells endowed with prompt commitment to Ig-secreting effectors, such as B1 B cells and marginal zone B-cells subsets (18). By applying the GEx differentially expressed genes signature to DLBCL we aimed at investigating whether the atypical status of

non-clonal germinotropic plasmablastic expansion could be represented in the transcriptional signature of a subset of DLBCL of either ABC or GCB COO. Previous reports described a subset of ABC-DLBCL expressing *PRDM1*/BLIMP1 and demonstrated that loss of function of this antigen is harbinger of a poor prognosis (19). Expression of IRF4/MUM1 is routinely employed in the diagnostic setting for the distinction of non-GC subtypes based on immunohistochemical algorithms (20). Moreover, specific subtypes of large B-cell lymphomas characterized by IRF4 rearrangement have been recently described and recognized as independent entities in the most recent WHO classification (21). We report additional molecular markers potentially associated with plasmablastic commitment in the GC, including the receptor of IL17B/IL25 IL17RB, the overexpression of which marks lymphoplasmacytic lymphomas with mutant $MYD88^{L265P}$ and $CXCR4^{WT}$ (22). In the GC setting, IL17B/IL25 signaling could enforce NF-κB activity (23) through TRAF6, which cooperation with CD40 signaling is required for B-cell affinity maturation and plasma cell differentiation (24). From the genes positively and negatively characterizing GEx ROIs, no relevant clues emerge about the mechanisms leading to the atypical GC retention and expansion of the plasmablastic elements. Under normal conditions, the suppression of Bach2 and Pax5 transcripts, along with the down-regulation of Bcl-6, IRF8 and PU-1 and the activation of BLIMP1 and MUM1/IRF4, drive the development of PCs resulting from the GC reaction (1). Once their effector/memory fate is established, B cells escape from the GCs through the suppression of the BCL-6-induced "confinement factor" S1PR2 and the expression of pro-migratory receptors that are likely to be involved in GC exit, such as EBI2 and S1PR1 (25). The downmodulation of lymphotoxin beta transcript emerging from the GEx ROIs profiling can imply an impaired activation of the FDC meshwork by resident elements (26) which would in turn impact on the maintenance of a functional GC microenvironment licensing atypical plasmablastic expansion within the GC contexture. Indeed, some cases of abrupt/florid follicular hyperplasia have been described in

303 which activated B cells are mainly localized in the GCs, partly twisting the normal follicular
304 architecture and even showing immunohistochemical light chain (oligoclonal) restriction,
305 leading to diagnostic concern for neoplasia (27). The evidence of a negative prognostic
306 significance of the GEx hallmark genes in a large harmonized dataset, which proved to be
307 significant in ABC but not in GCB cases, suggests that within the heterogeneous ABC COO,
308 in which specific genetic subgroups are enriched, GC-related proliferations of plasmablastic
309 elements could be represented. Genetic studies in such cases in which a dyscrasia between
310 cyto-architectural, phenotypical and topographic profile of a B-cell expansion with
311 plasmablastic/plasmacytic features may help in finding a link with specific genetic subsets of
312 DLBCL (28) and reconcile an ABC-COO with GC-like microenvironment features (29).
313
314

315 **Acknowledgements**

316 The Authors wish to acknowledge Prof. Maurilio Ponzoni for helpful discussion. This study
317 has been supported by the Italian Foundation for Cancer Research (AIRC) through the IG-2018
318 22145 Investigator Grant to C.T.; 5x1000 22759 Grant to C.T.; and by the Italian Ministry of
319 Education, University and Research (MIUR) grant 2017K7FSYB to C.T.

320
321
322

REFERENCES

1. De Silva NS, Klein U. Dynamics of B cells in germinal centres. Nat Rev Immunol. 2015 Mar;15(3):137-48. doi: 10.1038/nri3804. Epub 2015 Feb 6. PMID: 25656706; PMCID: PMC4399774.

2. Allen CD, Okada T, Cyster JG. Germinal-center organization and cellular dynamics. Immunity. 2007 Aug;27(2):190-202. doi: 10.1016/j.immuni.2007.07.009. PMID: 17723214; PMCID: PMC2242846.

3. Yam-Puc JC, Zhang L, Maqueda-Alfaro RA, Garcia-Ibanez L, Zhang Y, Davies J et al. Enhanced BCR signaling inflicts early plasmablast and germinal center B cell death. iScience. 2021 Jan 7;24(2):102038. doi: 10.1016/j.isci.2021.102038. PMID: 33532715; PMCID: PMC7822941.

4. Alizadeh AA, Eisen MB, Davis RE, Ma C, Lossos IS, Rosenwald A et al. Distinct types of diffuse large B-cell lymphoma identified by gene expression profiling. Nature. 2000 Feb 3;403(6769):503-11. doi: 10.1038/35000501. PMID: 10676951.

5. Chapuy B, Stewart C, Dunford AJ, Kim J, Kamburov A, Redd RA et al. Molecular subtypes of diffuse large B cell lymphoma are associated with distinct pathogenic mechanisms and outcomes. Nat Med. 2018 May;24(5):679-690. doi: 10.1038/s41591-018-0016-8. Epub 2018 Apr 30. Erratum in: Nat Med. 2018 Aug;24(8):1292. Erratum in: Nat Med. 2018 Aug;24(8):1290-1291. PMID: 29713087; PMCID: PMC6613387.

6. Schmitz R, Wright GW, Huang DW, Johnson CA, Phelan JD, Wang JQ et al. Genetics and Pathogenesis of Diffuse Large B-Cell Lymphoma. N Engl J Med. 2018 Apr 12;378(15):1396-1407. doi: 10.1056/NEJMoa1801445. PMID: 29641966; PMCID: PMC6010183.

7. Tripodo C, Zanardi F, Iannelli F, Mazzara S, Vegliante M, Morello G et al. A Spatially Resolved Dark- versus Light-Zone Microenvironment Signature Subdivides Germinal Center-Related Aggressive B Cell Lymphomas. iScience. 2020 Sep 16;23(10):101562. doi: 10.1016/j.isci.2020.101562. PMID: 33083730; PMCID: PMC7522121.

8. Ritchie ME, Phipson B, Wu D, Hu Y, Law CW, Shi W et al. Limma powers differential expression analyses for RNA-sequencing and microarray studies. Nucleic Acids Res. 2015 Apr 20;43(7):e47. doi: 10.1093/nar/gkv007. Epub 2015 Jan 20. PMID: 25605792; PMCID: PMC4402510.

9. Barrans SL, Crouch S, Care MA, Worrillow L, Smith A, Patmore R et al. Whole genome expression profiling based on paraffin embedded tissue can be used to classify diffuse large B-cell lymphoma and predict clinical outcome. Br J Haematol. 2012 Nov;159(4):441-53. doi: 10.1111/bjh.12045. Epub 2012 Sep 13. PMID: 22970711.

10. Sha C, Barrans S, Cucco F, Bentley MA, Care MA, Cummin T et al. Molecular High-Grade B-Cell Lymphoma: Defining a Poor-Risk Group That Requires Different Approaches to Therapy. J Clin Oncol. 2019 Jan 20;37(3):202-212. doi: 10.1200/JCO.18.01314. Epub 2018 Dec 3. Erratum in: J Clin Oncol. 2019 Apr 20;37(12):1035. PMID: 30523719; PMCID: PMC6338391.

11. Varano G, Raffel S, Sormani M, Zanardi F, Lonardi S, Zasada C et al. The B-cell receptor controls fitness of MYC-driven lymphoma cells via GSK3β inhibition. Nature. 2017 Jun 8;546(7657):302-306. doi: 10.1038/nature22353. Epub 2017 May 31. PMID: 28562582.

12. Tarte K, Zhan F, De Vos J, Klein B, Shaughnessy J Jr. Gene expression profiling of plasma cells and plasmablasts: toward a better understanding of the late stages of B-cell differentiation. Blood. 2003 Jul 15;102(2):592-600. doi: 10.1182/blood-2002-10-3161. Epub 2003 Mar 27. PMID: 12663452.

13. De Silva NS, Simonetti G, Heise N, Klein U. The diverse roles of IRF4 in late germinal center B-cell differentiation. Immunol Rev. 2012 May;247(1):73-92. doi: 10.1111/j.1600-065X.2012.01113.x. PMID: 22500833.

14. Sonja Boy, Marlene van Heerden, Roger Pool, Pascale Willem & Tomas Slavik. Plasmablastic lymphoma versus diffuse large B cell lymphoma with plasmablastic differentiation: proposal for a novel diagnostic scoring system. Journal of Hematopathology volume 8, pages 3–11 (2015). DOI 10.1007/s12308-014-0227-y.

15. O'Connor BP, Raman VS, Erickson LD, Cook WJ, Weaver LK, Ahonen C et al. BCMA is essential for the survival of long-lived bone marrow plasma cells. J Exp Med. 2004 Jan 5;199(1):91-8. doi: 10.1084/jem.20031330. PMID: 14707116; PMCID: PMC1887725.

16. Jourdan M, Caraux A, Caron G, Robert N, Fiol G, Rème T et al. Characterization of a transitional preplasmablast population in the process of human B cell to plasma cell differentiation. J Immunol. 2011 Oct 15;187(8):3931-41. doi: 10.4049/jimmunol.1101230. Epub 2011 Sep 14. PMID: 21918187.

17. Yoon SO, Zhang X, Lee IY, Spencer N, Vo P, Choi YS. CD9 is a novel marker for plasma cell precursors in human germinal centers. Biochem Biophys Res Commun. 2013 Feb 1;431(1):41-6. doi: 10.1016/j.bbrc.2012.12.102. Epub 2013 Jan 3. PMID: 23291167; PMCID: PMC3563937.

18. Won WJ, Kearney JF. CD9 is a unique marker for marginal zone B cells, B1 cells, and plasma cells in mice. J Immunol. 2002 Jun 1;168(11):5605-11. doi: 10.4049/jimmunol.168.11.5605. PMID: 12023357.

19. Xia Y, Xu-Monette ZY, Tzankov A, Li X, Manyam GC, Murty V et al. Loss of PRDM1/BLIMP-1 function contributes to poor prognosis of activated B-cell-like diffuse large B-cell lymphoma. Leukemia. 2017 Mar;31(3):625-636. doi: 10.1038/leu.2016.243. Epub 2016 Aug 29. PMID: 27568520; PMCID: PMC5837859.

20. Hans CP, Weisenburger DD, Greiner TC, Gascoyne RD, Delabie J, Ott G et al. Confirmation of the molecular classification of diffuse large B-cell lymphoma by immunohistochemistry using a tissue microarray. Blood. 2004 Jan 1;103(1):275-82. doi: 10.1182/blood-2003-05-1545. Epub 2003 Sep 22. PMID: 14504078.

21. Swerdlow, S.H.; Campo, E.; Harris, N.L.; Jaffe, E.S.; Pileri, S.A.; Stein, H. et al. WHO Classification of Tumours of Haematopoietic and Lymphoid Tissues, Revised 4th ed.; IARC: Lyon, France, 2017.

22. Hunter ZR, Xu L, Yang G, Tsakmaklis N, Vos JM, Liu X et al. Transcriptome sequencing reveals a profile that corresponds to genomic variants in Waldenström macroglobulinemia. Blood. 2016 Aug 11;128(6):827-38. doi: 10.1182/blood-2016-03-708263. Epub 2016 Jun 14. PMID: 27301862; PMCID: PMC4982454.

23. Maezawa Y, Nakajima H, Suzuki K, Tamachi T, Ikeda K, Inoue J et al. Involvement of TNF receptor-associated factor 6 in IL-25 receptor signaling. J Immunol. 2006 Jan 15;176(2):1013-8. doi: 10.4049/jimmunol.176.2.1013. PMID: 16393988.

24. Ahonen C, Manning E, Erickson LD, O'Connor B, Lind EF, Pullen SS et al. The CD40-TRAF6 axis controls affinity maturation and the generation of long-lived plasma cells. Nat Immunol. 2002 May;3(5):451-6. doi: 10.1038/ni792. Epub 2002 Apr 22. PMID: 11967542; PMCID: PMC2834483.

25. Green JA, Cyster JG. S1PR2 links germinal center confinement and growth regulation. Immunol Rev. 2012 May;247(1):36-51. doi: 10.1111/j.1600-065X.2012.01114.x. PMID: 22500830; PMCID: PMC3335345.

26. Myers RC, King RG, Carter RH, Justement LB. Lymphotoxin α1β2 expression on B cells is required for follicular dendritic cell activation during the germinal center response. Eur J Immunol. 2013 Feb;43(2):348-59. doi: 10.1002/eji.201242471. Epub 2012 Dec 5. PMID: 23112125; PMCID: PMC3753018.

27. Gars E, Butzmann A, Ohgami R, Balakrishna JP, O'Malley DP. The life and death of the germinal center. Ann Diagn Pathol. 2020 Feb;44:151421. doi: 10.1016/j.anndiagpath.2019.151421. Epub 2019 Nov 13. PMID: 31751845.

28. Wright GW, Huang DW, Phelan JD, Coulibaly ZA, Roulland S, Young RM et al. A Probabilistic Classification Tool for Genetic Subtypes of Diffuse Large B Cell Lymphoma with Therapeutic Implications. Cancer Cell. 2020 Apr 13;37(4):551-568.e14. doi: 10.1016/j.ccell.2020.03.015. PMID: 32289277.

29. Kotlov N, Bagaev A, Revuelta MV, Phillip JM, Cacciapuoti MT, Antysheva Z et al. Clinical and Biological Subtypes of B-cell Lymphoma Revealed by Microenvironmental Signatures. Cancer Discov. 2021 Jun;11(6):1468-1489. doi: 10.1158/2159-8290.CD-20-0839. Epub 2021 Feb 4. PMID: 33541860; PMCID: PMC8178179.

FIGURE LEGENDS

Figure 1

A, Digitalized slide selection of the Haematocylin and Eosin (H&E)-stained section of the tonsil highlighting the presence of an aberrantly expanded germinal center (asterisk) characterized by the presence of elements with plasmacytoid morphology (inset). On the H&E, representative regions relative to germinal center dark zone (DZ) and light zone (LZ) areas, peri-follicular (Peri) areas, and germinotropic plasmablastic expansion (GEx) areas, are highlighted. Original magnification x50. **B**, Comparative analysis of H&E and IHC for Bcl-2, Bcl-6, CD3, CD20, Kappa and Lambda light chain, Ki67, IRF4, IRF4/CD10, CD2, CD138 in the DZ, LZ, Peri and GEx areas highlighted in A. **C,** Heatmap of the average expression of the quantitative immunohistochemical analysis of the markers evaluated in the DZ, LZ, Peri, and GEx areas highlighted in B.

Figure 2

A, Two-dimensional principal component reduction of the DZ (n=5), LZ (n=5), Peri (n=5), and GEx (n=9) regions of interest (ROIs) profiles according to Digital Spatial Profiling of 1824 genes. **B**, Unsupervised hierarchical clustering of the 24 ROIs. **C**, Venn diagram of UP-modulated genes from three different comparisons (i.e., GEx vs DZ, GEx vs LZ, and GEx vs Peri). **D**, Venn diagram of DOWN modulated genes from three different comparisons (i.e., GEx vs DZ, GEx vs LZ, and GEx vs Peri). **E**, GEx signature genes. These genes are significantly differentially expressed in GEx in each comparison. **F**, Heatmap of differentially expressed genes in GEx as compared to DZ, LZ and Peri ROIs. The GEx signature shows a high discriminatory capacity between GEx ROIs and the other regions.

Figure 3

A, Unsupervised clustering analysis of the 1147 DLBCL cases based on the GEx signature. The signature identifies two distinct clusters; the blue one is characterized by a higher gene expression, while a lower gene expression characterizes the green one. **B**, Survival analysis on the two groups of DLBCL cases obtained from the unsupervised clustering. The overall survival is significantly lower in the group characterized by the higher GEx signature expression. The inset panel reports the cumulative distributions of the total GEx signature expression per patient in the two groups (Kolmogorov-Smirnov p-value < 10e-10). **C**, Survival analysis on the two groups – Q1 and Q4 - of DLBCL cases selected according to the cumulative distribution of the total GEx signature. The first and the fourth quartiles identify the Q1 and Q4 groups, respectively. **D**, Survival analysis on the Q1 and Q4 groups of ABC-DLBCL cases. **E**, Survival analysis on the Q1 and Q4 groups of GCB-DLBCL cases.

Figure 1

A

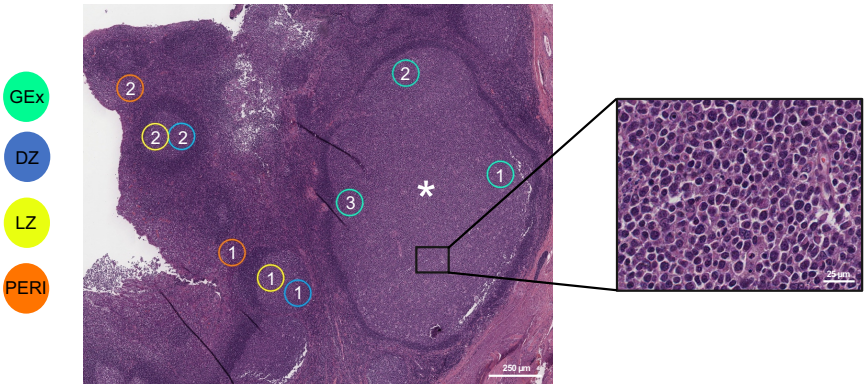

B

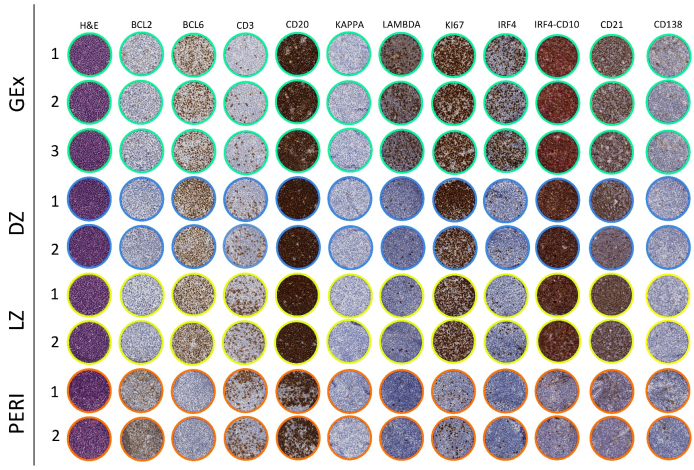

C

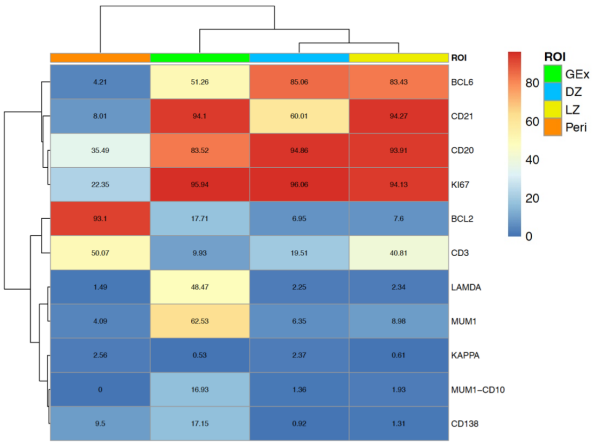

503

Figure 2

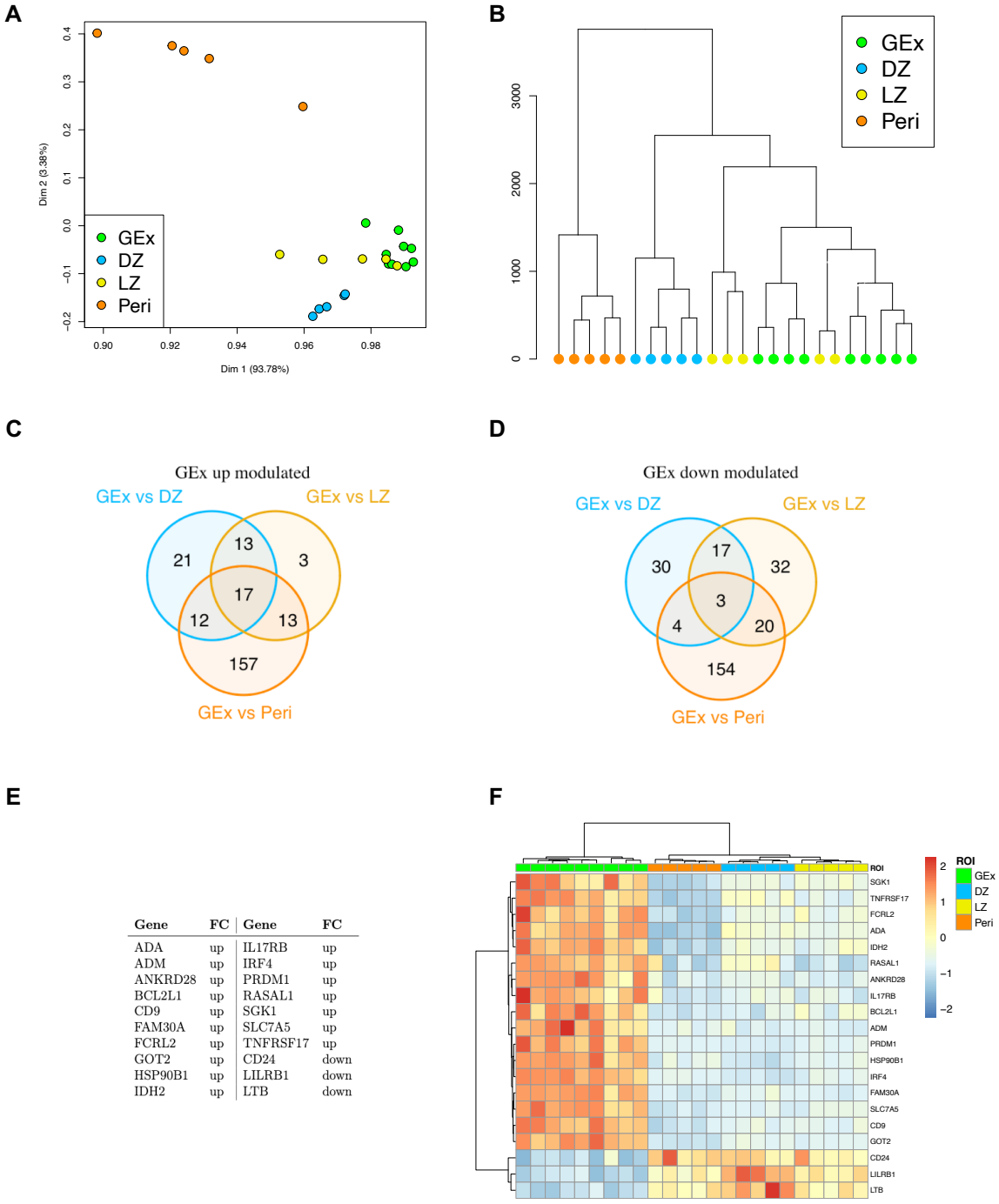

Gene	FC	Gene	FC
ADA	up	IL17RB	up
ADM	up	IRF4	up
ANKRD28	up	PRDM1	up
BCL2L1	up	RASAL1	up
CD9	up	SGK1	up
FAM30A	up	SLC7A5	up
FCRL2	up	TNFRSF17	up
GOT2	up	CD24	down
HSP90B1	up	LILRB1	down
IDH2	up	LTB	down

504

Figure 3

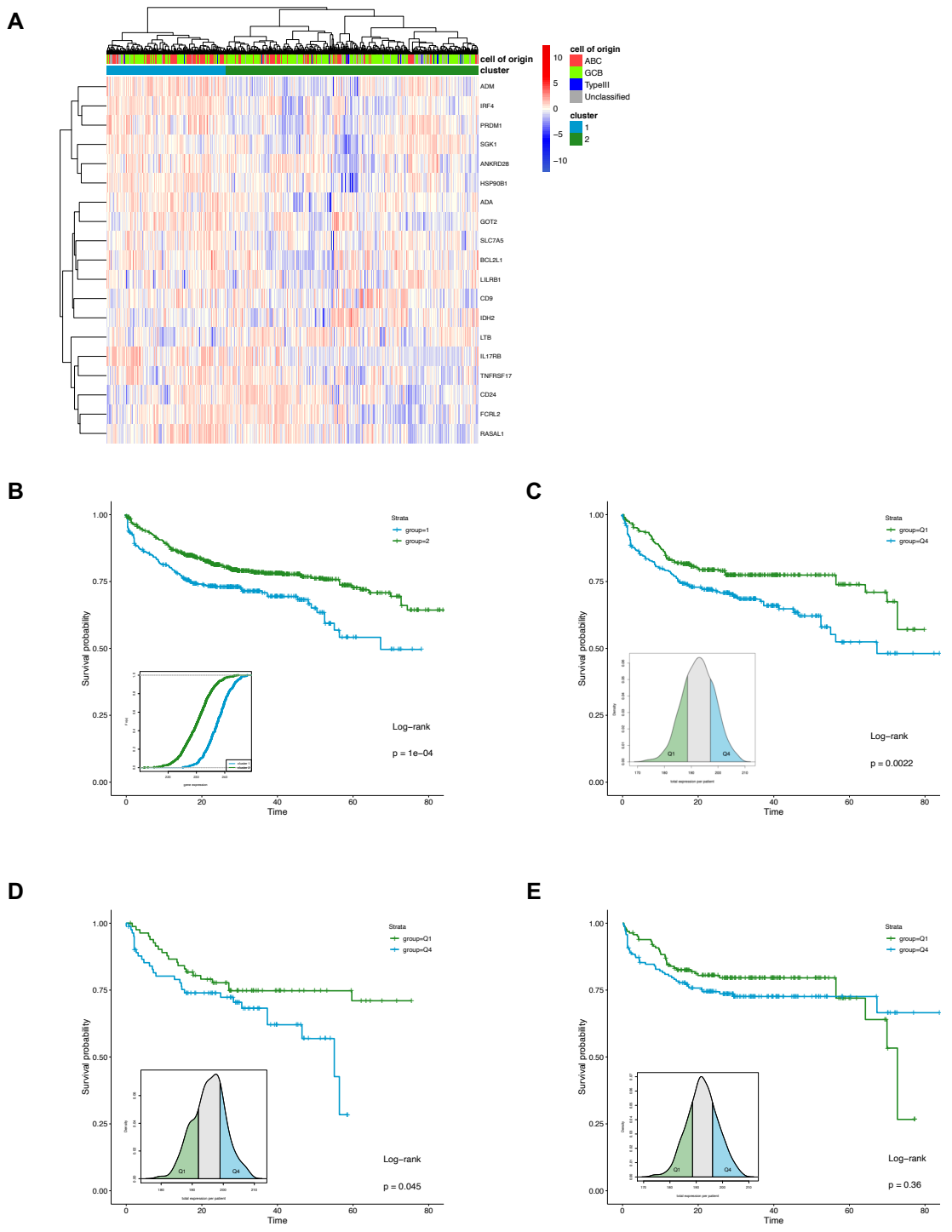

505